Geological Magazine

www.cambridge.org/geo

Multi-phase ecological change on Indian subcontinent from the late Miocene to Pleistocene recorded in the Nicobar Fan

Brian House[1,2], Kevin T. Pickering[3] and Richard Norris[1]

[1]Scripps Institution of Oceanography, La Jolla, CA, USA; [2]Department of Earth, Planetary, and Space Science, University of California Los Angeles, Los Angeles, CA, USA and [3]Department of Earth Sciences, University College London (UCL), London, UK

Original Article

Cite this article: House B, Pickering KT, and Norris R. Multi-phase ecological change on Indian subcontinent from the late Miocene to Pleistocene recorded in the Nicobar Fan. *Geological Magazine* https://doi.org/10.1017/S0016756823000481

Received: 9 December 2022
Revised: 11 July 2023
Accepted: 17 July 2023

Keywords:
C_4 expansion; palaeoclimate; Miocene climate; IODP; C_3-C_4; Indian subcontinent

Corresponding author:
Kevin T. Pickering;
Email: kt.pickering@ucl.ac.uk

Abstract

Modern grasslands on the Indian subcontinent, North and South America, and East Africa expanded widely during the late Miocene – earliest Pleistocene, likely in response to increasing aridity. Grasses utilizing the C_4 photosynthetic pathway are more tolerant of high temperatures and dry conditions, and because they induce less C isotope fractionation than plants using the C_3 pathway, the expansion of C_4 grasslands can be traced through the $\delta^{13}C$ of organic matter in soils and terrigenous marine sediments. We present a high-resolution record of the elemental and isotopic composition of bulk organic matter in the Nicobar Fan sediments from IODP Site U1480, off western Sumatra, to elucidate the timing and pace of the C_3–C_4 plant transition within the ~1.5×10^6 km^2 catchments of the Ganges/Brahmaputra river system, which continue to supply voluminous Himalaya-derived sediments to the Bay of Bengal. Using a multi-proxy approach to correct for the effects of marine organic matter and account for major sources of uncertainty, we recognize two phases of C_4 expansion starting at ~7.1 Ma, and at ~3.5 Ma, with a stepwise transition at ~2.5 Ma. These intervals appear to coincide with periods of Indian Ocean and East Asian monsoon intensification, as well as the expansion of Northern Hemisphere glaciation starting at ~2.7 Ma. Our data from the deep sea for a multi-phased C_4 expansion on the Indian subcontinent are in agreement with terrestrial data from the Indian Siwaliks.

1. Introduction

The Neogene expansion of C_4 vegetation represented a major reorganization of the Earth's terrestrial biome. In many parts of the world, after ~20 million years, the late Miocene (~11–5 Ma) witnessed the establishment of grasslands dominated by grass species using the C_4 photosynthetic pathway (Edwards *et al.* 2010; Polissar *et al.* 2021). Distinct carbon isotopic values of C_3 and C_4 plants are widely used to reconstruct past hydroclimate, where wetter conditions are associated with more abundant C_3 plants, and drier conditions by greater C_4 coverage (e.g. Kirkels *et al.* 2022*a*, *b*). Using the premise that plant-derived material retains the carbon isotopic signature of its photosynthetic pathway during transfer from plant to sediment, we analysed the isotopic composition of organic carbon (OC) preserved in deep-marine sediments from the Nicobar Fan as a proxy for palaeo-environmental change. We use these carbon isotopes to investigate likely long-term changes in the hydroclimate of the sediment source area for the Middle Miocene-Pleistocene Nicobar Fan, Indian Ocean. In particular, we analysed the finer-grained sediments (mudstones) from the siliciclastic Nicobar Fan as fluvial transport of fine particles generally leads to the enrichment of OC and their effective offshore transport as suspended load (e.g. Bianchi *et al.* 2018).

Shortly after 10 Ma, a major palaeoclimate transition appears to have led to a synchronous expansion of grasslands on the Indian subcontinent as well as in East Africa and North and South America (e.g. Cerling *et al.* 1997). Evidence for this comes from the C isotopic composition of tooth enamel (Cerling *et al.* 1997), palaeosol carbonate nodules (Quade *et al.* 1989; Freeman and Colarusso, 2001; Karp *et al.* 2018), terrestrial sediments (Vögeli *et al.* 2017) and terrigenous marine sediments (Freeman & Colarusso, 2001). All of these record a shift towards higher $\delta^{13}C$ values that suggest an expansion of vascular plants utilizing the more complex C_4 photosynthetic pathway rather than the C_3 pathway of woody plants, marine photosynthesizers and many grasses. Because the C_4 pathway produces a lower degree of C isotopic fractionation, the increase in $\delta^{13}C$ of both bulk organic matter and terrestrial biomarkers is interpreted to reflect the expansion of C_4 plants, most of which are grasses, and are better suited than C_3 plants to warmer and more arid conditions. The expansion of C_4 plant coverage in the late Miocene is therefore interpreted to be an indication of increasing aridity (e.g. Quade *et al.* 1989; Cerling *et al.* 1997; Freeman & Colarusso, 2001; Zhisheng *et al.* 2001; An *et al.* 2005; Scheiter *et al.* 2012; Karp *et al.* 2018; Khim *et al.* 2020; Morley, 2018), but it should

also be noted that because the C_4 pathway involves a CO_2 preconcentration mechanism, low atmospheric pCO_2/pO_2 will additionally favour C_4 grassland expansion (Cerling *et al.* 1997). In a study of past vegetation patterns in the Indian Siwaliks (middle and lower Gangetic Plain), Basu *et al.* (2015) concluded that the early appearance of C_4 plants occurred at ~11 Ma. Also, from an analysis of the $\delta^{13}C$ values of bulk soil organic matter, n-alkane and n-alkanoic acid in the palaeosols from Late Mio-Pleistocene Siwaliks, Roy *et al.* (2020) identified two phases of vegetation change between at ~7 Ma and at ~3 Ma – an expansion of C_4 plants during 7–3 Ma and a higher abundance of C_3 plants after 3 Ma. They invoked a morpho-tectonic control for these changes in vegetation.

The late Miocene expansion of C_4 vegetation has been considered as globally synchronous, but site-specific studies reveal differences in the timing of this expansion and suggest that local conditions played an important role (e.g. Dunlea *et al.* 2020; Tauxe & Feakins, 2020). Data from marine sediments, since ~6 Ma in the Bay of Bengal at IODP Site U1445, led Dunlea *et al.* (2020) to propose that C_4 vegetation on the Indian Peninsula existed before the end of the Miocene but expanded to substantially greater abundance during the mid-Pliocene to mid-Pleistocene (~3.5–1.5 Ma). In this paper, we also identify the ~3.5–1.5 Ma expansion (see below). Tauxe and Feakins (2020) re-evaluated the constraints for the carbon isotopic shifts recorded from the Indian subcontinent and demonstrated a diachronous transition ranging in age from ~7.8 Ma in Pakistan to as late as ~6 Ma in Nepal. The record from IODP Expedition 355 Site U1457, drilled on the Indus Fan, shows that the transition in peninsular India began at ~7.2 Ma, with similar records from the African margin witnessing an earlier shift to C_4 dominance starting at ~10 Ma, with those from Australia and South America during the Pliocene. They argued that diachroneity in vegetation changes around the globe does not invalidate pCO_2 as a driver but is consistent with it being one of several drivers of the global C_4 expansion.

The Indian subcontinent has received particular attention regarding the C_3–C_4 transition in part because of the potential relationship between vegetation and monsoon intensity. The strength of monsoon winds is a fundamental control on aridity on the Indian subcontinent where southwesterly winds in summer bring moisture-laden air from the Arabian Sea and northern Indian Ocean inland. Humid air masses deflected upwards by the Himalaya cause extreme precipitation compared to the dry winters in which northeasterly winds provide little moisture. The separate East Asian monsoon system, while not as pronounced, leads to similar intra-annual precipitation patterns in Central and East Asia. Even if intensification of either monsoon system does not lead to an overall increase in annual precipitation, an increase in summer precipitation, particularly with the trade-off of greater winter aridity, will tend to favour C_4 grasses (An *et al.* 2005), which are better suited to warm and dry conditions due to their ability to limit water loss during stomatal gas exchange. The intensity of monsoonal winds has also been inferred from marine productivity, which strengthens upwelling off the Arabian Peninsula during the summer monsoon (Kroon *et al.* 1991; Prell & Kutzbach. 1992), and dust flux proxies (Rea *et al.* 1998; Wan *et al.* 2007).

Terrestrial records of monsoon intensity tend to reflect local conditions, which means they may not be representative of continental-scale ecological shifts (Freeman & Colarusso, 2001; Vögeli *et al.* 2017). Much of the evidence for grassland expansion has come from the Siwalik palaeosols in northern Pakistan and India (Fig. 1), and despite efforts to sample throughout the spatial extent of this unit (e.g. Freeman & Colarusso, 2001; Vögeli *et al.* 2017), extrapolating regional results from a single geologic unit can introduce substantial uncertainty. Other efforts to understand long-term climate evolution on the Indian subcontinent have focused on the elemental and isotopic composition of organic matter in terrigenous sediments of the Indus and Bengal Fans (Freeman & Colarusso, 2001; Krishna *et al.* 2013; Karp *et al.* 2018; Khim *et al.* 2020), which integrate ecological signals over entire river catchments, and can therefore better capture large-scale environmental changes with less interference from spatial heterogeneity. Clift *et al.* (2008) used weathering records from the South China Sea, Bay of Bengal and Arabian Sea to propose that over the past 23 million years, there has been a dynamic coupling between Neogene climate and both erosion and deformation in the Himalaya, that is, a strong tectonic control.

2. Sediment sources

The Bengal–Nicobar Fan system (Figs. 1, 2), which is uniquely suited to address climate evolution in South Asia because of the largely continuous record of terrigenous sediment flux to the deep sea since 10 Ma and the extremely high sediment accumulation rates (McNeill *et al.* 2017*a*, *b*; Pickering *et al.* 2019, 2020), also observed in the Bengal Fan (Lee *et al.* 2019). Submarine fan deposits at IODP Site U1480 are largely the result of various types of sediment gravity flows (SGFs) of Himalaya-sourced material transported via the Ganges/Brahmaputra river system (Pickering *et al.* 2019, 2020; Chen *et al.* 2020) and therefore incorporate terrigenous organic matter from the combined catchment area. Petrographic data, including geochemical analyses, all support a single and sustained major sediment provenance to the north from the Himalaya and surrounding areas for the entire time interval cored in the Nicobar Fan (McNeill, Dugan, Petronotis, and the Expedition 362 Scientists, 2017b; McNeill *et al.* 2017a; also see section on provenance in Pickering *et al.* 2019). Arc-derived ash content in sediments at IODP Sites U1480-U1481 suggests that the Sunda forearc contributed only a very minor component. Geochemical and Sr-Nd isotope analyses on the bulk silicate fraction of the Nicobar Fan muds/mudstones indicate an eastern Himalayan source dominated by the Greater Himalaya, with a significant Gangdese arc contribution (a major geological structure in the southern Tibetan Lhasa terrane to the north of the Himalayas), all primarily carried by the palaeo-Brahmaputra river. Thus, we are confident that the mudstones sampled for this study are part of this terrigenous sediment flux from the Himalaya, and not from a separate source area to the east, such as the Irrawaddy drainage system.

The Bengal–Nicobar Fan system contains large amounts of woody material. Rapid export and burial of woody material is a highly efficient pathway of atmospheric CO_2 sequestration (Lee *et al.* 2019). Large-magnitude, low-frequency rapid wood transport avoids degradation that can occur in soils, where extensive OC degradation limits the efficiency of OC burial at very high erosion rates (*ibid.*).

Palaeogeographic reconstructions of the Bengal–Nicobar Fan System, using the plate-tectonic reconstructions of Hall (2012), with the Bengal Fan morphology from Curray (2014), combined with core data from DSDP/ODP/IODP sites in the Indian Ocean (Fig. 2 modified from Pickering *et al.* 2019), suggest that the earliest submarine-fan deposits likely were routed along the eastern side of the Indian Ocean, as axial SGFs along the Sunda subduction zone trench that would have been a linear topographic low until it was

https://doi.org/10.1017/S0016756823000481 Published online by Cambridge University Press

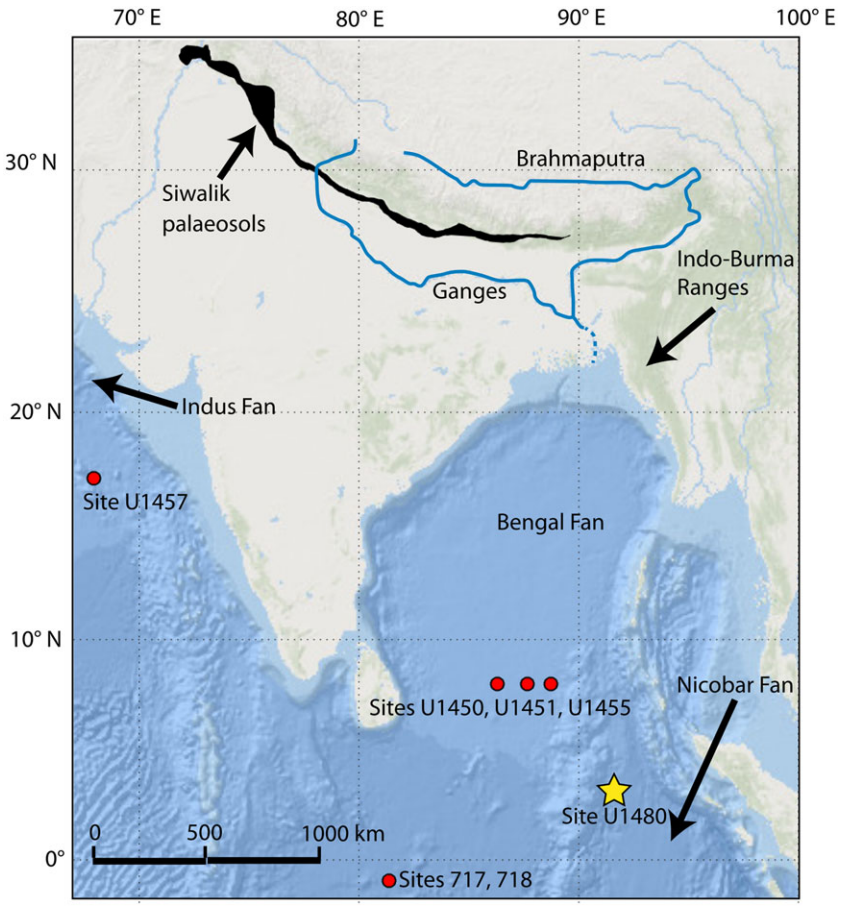

Figure 1. (Colour online) Overview map showing the location of IODP Site U1480 on the Nicobar Fan and sites where other related studies have been conducted. The Ganges and Brahmaputra rivers provide most of the terrigenous sediment to the Nicobar and Bengal Fans (the approximate position of the river system near the Bay of Bengal is denoted as the delta is complex). Palaeosols of the Siwalik group are the most studied terrestrial deposits that provide evidence for the C_3–C_4 shift, though no shift appears to have occurred at the eastern extent of the group, and it captures conditions at the foot of the Himalaya, not farther into the lowlands where C_4 grasses may be expected to first appear (Freeman & Colarusso, 2001).

overfilled to construct the Bengal–Nicobar Fan System. For a comprehensive explanation of SGFs, see Pickering and Hiscott (2016). The latest Eocene and early Oligocene Andaman Flysch, now as accreted and uplifted sedimentary rocks forming part of the Andaman Islands, represents the oldest trench deposits (Pickering *et al.* 2019, Figure 14). There was a substantially increased delivery of coarser-grained terrigenous sediment to the Bengal–Nicobar Fan System between 13.5 and 8.5 Ma (but beginning at ~27 Ma), switching to the Nicobar Fan after ~9.5–9.0 Ma, and then back to the Bengal Fan after ~2 Ma (Pickering *et al.* 2020, Figure 14). High elevation in the evolving Tibetan Plateau (>4 km), starting at ~55–45 Ma, appears to have been established by ~20 Ma (Ding *et al.* 2022) and, therefore, this was likely an important sediment source to the Nicobar Fan before the time interval considered in this paper.

Although IODP Site U1480 is ~2,000 km from the sediment source in the Bay of Bengal, sediment accumulation rates were commonly higher than at IODP sites on the distal Bengal Fan (Fig. 1). Additionally, the IODP Site U1480 record more fully captures the depositional history since ~10 Ma with fewer hiatuses, intervals of bit advancement without coring and better age constraints than many of the Bengal and Indus Fan sites (IODP sites U1450, U1451, U1455 and U1457; Expedition 354 Scientists, 2016*a*, *b*, *c*; Khim *et al.* 2020). Site U1480, therefore, represents a unique opportunity to capture a largely continuous record of ecologic and palaeoclimate conditions during the past ~10 Ma on the Indian subcontinent.

Our datasets give a unique view of the timing and pace of the C_3–C_4 transition. While previous studies relied primarily on compound-specific isotope analyses of terrestrial plant biomarkers (e.g. Freeman & Colarusso, 2001), we instead used simple analytical techniques to generate a much larger dataset capable of revealing more subtle temporal trends and reduce the reliance on single measurements. Because the incorporation of organic matter from the marine ecosystem can mimic a shift towards terrestrial C_4 plant cover (e.g. Galy *et al.* 2008), we employed a multi-proxy approach that used mixing models based on $\delta^{13}C$, TOC/TN and Br/TOC ratios to correct for contributions from marine organic matter. Uncertainty in end-member composition can dramatically limit the utility of mixing models, so we used Monte Carlo simulations using randomly perturbed end-member compositions to place reasonable quantitative bounds on the contributions of C_4 plants to the terrigenous organic matter through time.

3. Methods

3.a. Analytical procedures

The sample set consists of the residues from shipboard carbonate/TOC analyses and additional dedicated samples that were vacuum sealed and kept frozen. These samples came from the muds/mudstones in the Nicobar Fan sediments (Units I–IIIA in IODP Site U1480 (0–1,310.02 mbsf) and are representative of the siliciclastic sediments in the Nicobar Fan). An analysis of siliciclastic sediments from the Indus Fan (Arabian Sea) has already established that hemipelagic mudstones (rather than sands deposited from various SGFs, such as turbidity currents) provide the most suitable

https://doi.org/10.1017/S0016756823000481 Published online by Cambridge University Press

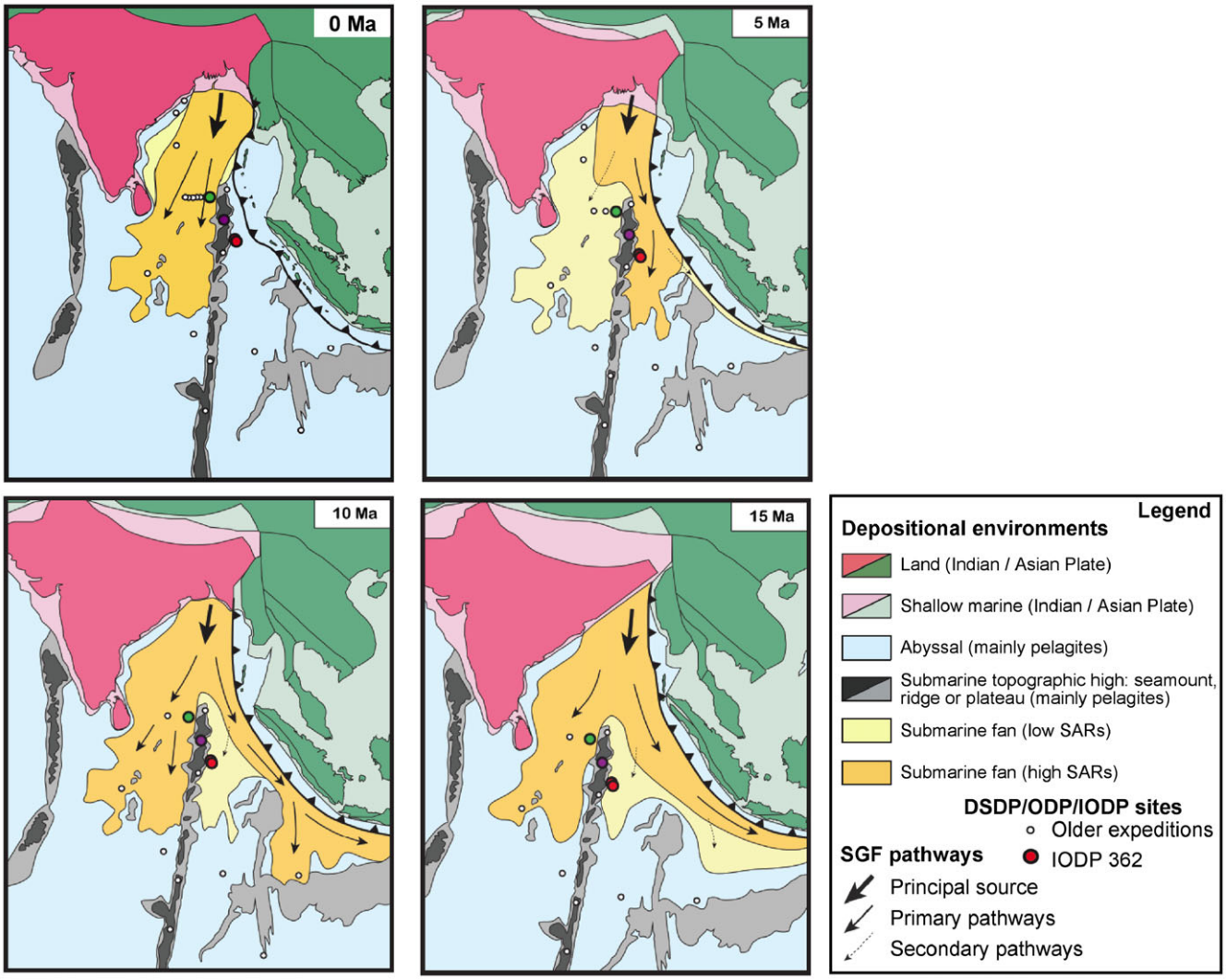

Figure 2. (Colour online) Palaeogeographic reconstructions of the Bengal–Nicobar Fan System for the time interval 0–10 Ma, modified from Pickering *et al*. (2019). Tectonic reconstruction used is from Hall (2012). Bengal Fan morphology from Curray (2014). Location of core data from DSDP/ODP/IODP sites (white dots; red dots = IODP Expedition 362 sites). Sediment mass accumulation rates (MARs) were calculated for IODP sites U1451 (green dot), U1453 (purple dot) and U1480-U1481 (red dots): the white dots are other drill DSDP/ODP/IODP sites. The postulated earliest submarine-fan deposits are shown as routing along the eastern side of the Indian Ocean, as axial sediment gravity flows along the Sunda subduction zone trench until it was overfilled to construct the Bengal Fan. The latest Eocene and early Oligocene Andaman Flysch, now as accreted and uplifted sedimentary rocks forming part of the Andaman Islands, is the oldest interpreted trench deposits (~30 Ma). Also, note the much increased coarser-grained terrigenous sediment supply to the Bengal Fan between 13.5 Ma and 8.5 Ma (but beginning at ~27 Ma), switching to the Nicobar Fan after ~9.5–9.0 Ma and then back to the Bengal Fan after ~2 Ma.

material for evaluating any changes in C_4 grasses (Feakins *et al.* 2020). The carbonate residues were freeze-dried for 12 hours, while additional dedicated samples were dried at 50°C until consecutive weighing indicated no further mass loss. All samples were ground in an agate mortar and pestle. Approximately 10 mg of sediment was weighed into Ag capsules and decarbonated for TOC and $\delta^{13}C$ analyses using aqueous SO_2 (~6–8% by mass). Following dropwise addition of SO_2 solution, the samples were heated to 60°C until dry, at which point additional SO_2 solution was added. We continued this procedure until a total of ~1.5 mL had been added, representing at least a 100-fold stoichiometric excess of SO_2/$CaCO_3$. Pre-combusted glass pipettes and polypropylene 96-well plates were used to minimize any possibility of contamination with organic matter during decarbonation. The Ag capsules containing the decarbonated sediment samples were sealed in Sn capsules to aid in final conversion of organic C to CO_2 in the elemental analyser combustion column. Separate sample aliquots of ~40 mg were not subjected to decarbonation and were sealed in Sn capsules for TN analyses.

Prior results (Kennedy *et al.* 2005) suggested that aqueous SO_2 incompletely decarbonates samples for TOC analysis, but the amount of SO_2 solution added provided a less than stoichiometric ratio of $SO_2/CaCO_3$, so decarbonation should not proceed to completion. Because our samples were likely to contain trace detrital dolomite ($(Ca,Mg)CO_3$), which is resistant to decarbonation, and would artificially raise $\delta^{13}C_{TOC}$ measurements, we tested the decarbonation procedure on a powdered dolomite sample from the Scripps Institution of Oceanography collections. The C content of the untreated dolomite implies an Mg concentration of ~33%, and decarbonation of ~1 mg, far in excess of the amount in our samples, resulted in C concentrations below the analytical detection limit of <10 ug C. We are therefore confident that the

https://doi.org/10.1017/S0016756823000481 Published online by Cambridge University Press

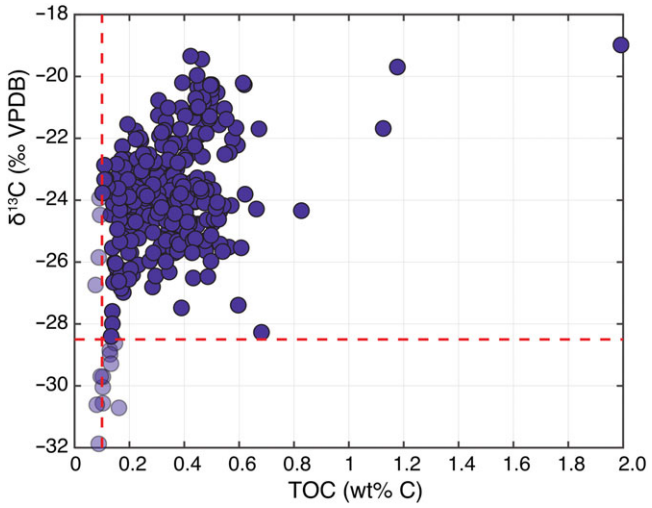

Figure 3. (Colour online) Measured $\delta^{13}C_{TOC}$ as a function of TOC in IODP Site U1480 sediments shows a substantial decrease in $\delta^{13}C_{TOC}$ in samples with low TOC. The positions of the red lines indicate the cut-offs used to filter data (Section 4.1); points to the left and below these lines were not used for further analyses.

decarbonation procedure we used quantitatively removes even unrealistically large amounts of $(Ca,Mg)CO_3$ and is suitable for analysing TOC and $\delta^{13}C_{TOC}$. Decarbonation with aqueous SO_2 has the added benefit of producing Ca/Mg salts that are not hygroscopic, obviating the need for the rigorous drying procedures required after decarbonation by HCl fumigation.

Analyses of TOC, $\delta^{13}C$ of TOC ($\delta^{13}C_{TOC}$) and TN were conducted at the University of California Santa Cruz Stable Isotope Laboratory. Carbon and nitrogen isotopic and elemental composition were determined by Dumas combustion using a Carlo Erba 1108 elemental analyser coupled to a ThermoFinnigan Delta Plus XP isotope ratio mass spectrometer. Analytical precision of internationally calibrated in-house standards is better than 0.2 ‰ for $\delta^{13}C$, which means the $\delta^{13}C$ error bars in Figs. 3–5 would be smaller than the data points. Sample isotopic values are corrected for size, drift and source stretching effects. Carbon and nitrogen elemental composition is calculated based on standards of known elemental composition. Precision of these known compounds is determined to be better than 1%, again indicating error bars smaller than data points in Fig. 3. All $\delta^{13}C$ values are reported relative to the Vienna Pee Dee Belemnite (VPDB) C isotope standard.

Major and trace element analyses were conducted on sample aliquots that were washed three times with DI water and centrifuged between washings to ensure seawater-derived bromide would not interfere with sediment Br measurements. The sample aliquots were analysed by Instrumental Neutron Activation Analysis (INAA) at the Oregon State University Radiation Center. Precision is estimated at ~0.7 ppm at the 2σ level for Br, and we also used this value as the detection limit.

3.b. Data treatment

Data were first filtered to address the tendency for samples with low TOC to give low $\delta^{13}C$ values (Fig. 3). We established a cut-off of 0.125 wt% C and an overall $\delta^{13}C$ threshold of −28.5 to discard unreliable data while still retaining as many as possible. For Br analyses, we discarded data points for samples with over 400 ppm Cl, which may indicate incomplete removal of seawater Br based on co-variation between Br and Cl for samples with high Cl content. Furthermore, data for which Br concentrations were less than two standard deviations from the detection limit of 0.7 ppm were also discarded. These procedures led to 302 measurements of TOC, $\delta^{13}C_{TOC}$ and TN as well as 28 measurements of Br (and other major/trace elements) that we deemed to be reliable (Tables S1; S2). Only these data were used in further analyses.

We used two separate three end-member mixing models to correct the $\delta^{13}C_{TOC}$ values for the influence of marine organic matter and place quantitative bounds on the fraction of organic matter from C_4 plants. Both consisted of a system of linear equations of the form $Af = b$ where $A = \begin{bmatrix} c^1_{C4} & c^1_{C3} & c^1_M \\ c^2_{C4} & c^2_{C3} & c^2_M \\ 1 & 1 & 1 \end{bmatrix}$ with c^i_j equal to the composition of end-member j with respect to the elemental/isotopic system i, $f = \begin{bmatrix} f_{C4} \\ f_{C3} \\ f_M \end{bmatrix}$ with the fractional contribution f_j from end-member j and $b = \begin{bmatrix} d^1_1 & d^1_2 & \dots \\ d^2_1 & d^2_2 & \dots \\ 1 & 1 & \dots \end{bmatrix}$ with data d^i_k for the measured value of data point k with respect to the elemental/isotopic system i. A total of 10^5 Monte Carlo simulations were run in which end-member compositions were allowed to vary randomly within distributions centred on literature values (e.g. Galy *et al.* 2008) and/or extreme measured values and with standard deviations encompassing a range of reasonable values (Table 1). The distributions of $\frac{f_{C4}}{f_{C4}+f_{C3}}$ (the fraction of terrigenous organic matter from C_4 plants) are represented in Fig. 6, and we generated smoothed curves fitting the data based on the distributions produced by bootstrap resampling of the data and the smoothed values at ages corresponding to those of the data.

4. Results and discussion

4.a. Correcting for marine organic matter inputs

Bulk TOC $\delta^{13}C$ data have been shown to correlate well with C isotope ratios of terrestrial plant biomarkers in Bengal Fan sediments (Freeman & Colarusso, 2001; Galy *et al.* 2008), suggesting that marine sediment $\delta^{13}C_{TOC}$ (Fig. 3) presents a reasonable first-order view of landscape evolution and therefore palaeoclimate conditions. However, because the $\delta^{13}C$ values of marine organic matter are typically intermediate between those of vascular C_3 and C_4 plant material, a shift towards higher $\delta^{13}C$ values could reflect greater marine organic matter input rather than a true shift towards greater C_4 plant abundance. Attempting to remove the marine organic matter $\delta^{13}C$ signal using only $\delta^{13}C_{TOC}$ results in a mathematically underdetermined system in which the mixing contributions of three end-members (C_3, C_4 and marine organic matter) cannot be uniquely defined. Because correcting for inputs from marine organic matter offers the potential to place at least quantitative bounds on the C_3/C_4 contributions, we applied a multi-proxy approach to reduce the influence of marine organic matter contributions.

The ratio of TOC to total nitrogen (TN) is a widely used metric for the fraction of marine organic matter in marine sediments because while terrestrial organic C preserved in sediment is generally N-poor, largely proteinaceous marine organic matter tends to have much greater TN, leading to high TOC/TN ratios for terrigenous and low TOC/TN ratios for marine organic matter

https://doi.org/10.1017/S0016756823000481 Published online by Cambridge University Press

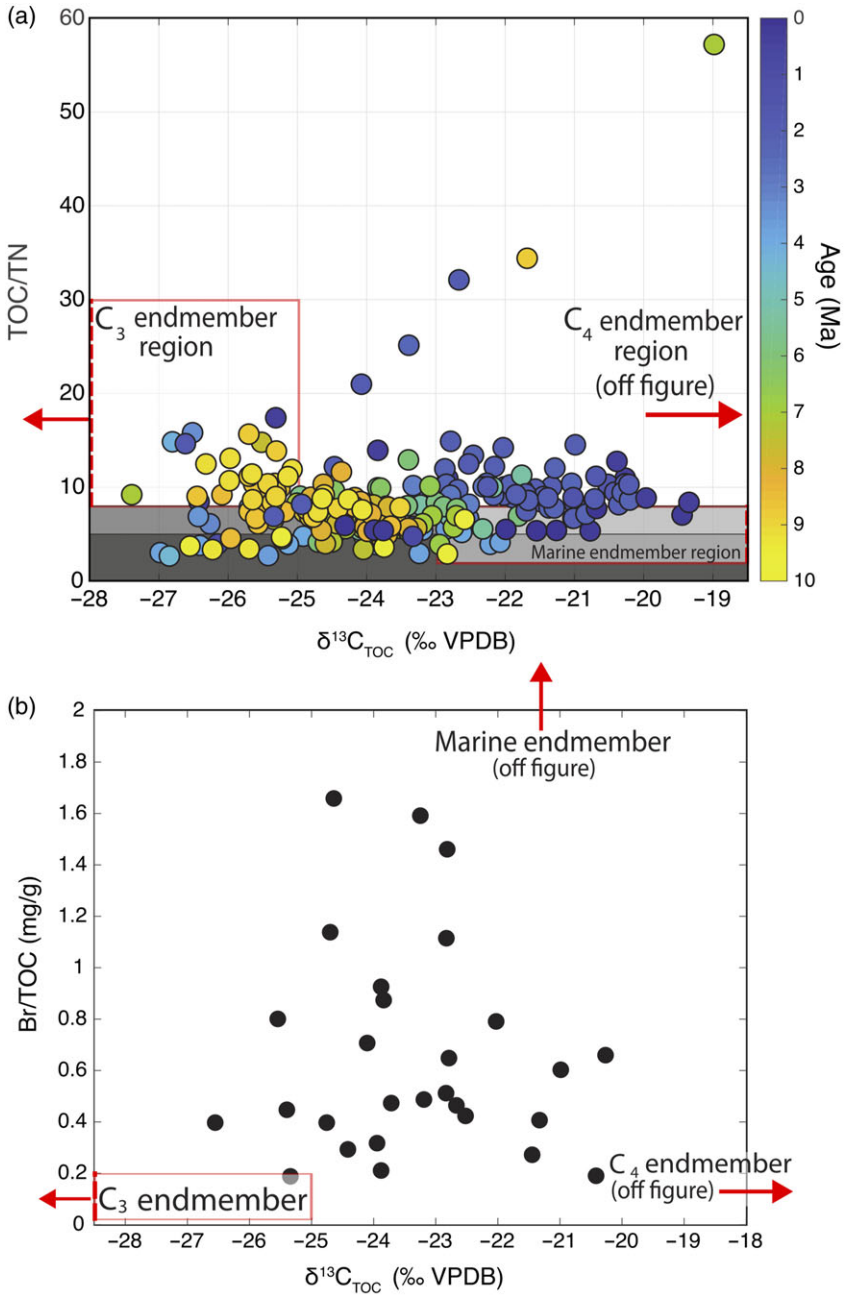

Figure 4. (Colour online) $\delta^{13}C_{TOC}$ and TOC/TN data (a) can be largely explained by a mixing model between organic matter from vascular C_3 plants with high TOC/TN and low $\delta^{13}C$, C_4 plants with high TOC/TN and high $\delta^{13}C$, and marine organic matter with low TOC/TN and intermediate $\delta^{13}C$. Shaded regions indicate the approximate TOC/TN range of <5–8 for marine organic matter and >8 for both C_3 and C_4 terrestrial organic matter. The $\delta^{13}C_{TOC}$ and Br/TOC data (b) are consistent with the three end-member mixing models introduced by Mayer *et al.* (2007) in which terrigenous organic matter is characterized by much lower Br/TOC ratios than marine organic matter. Note that many end-member regions exist or extend off margin of figure as indicated by red arrows. See Table 1 to appreciate the end-member regions.

(Fig. 5). However, TOC/TN as an organic matter provenance proxy suffers from several problems, most notably the potential for inorganic N (primarily as NH_4^+) to adsorb to clay minerals, producing artificially low TOC/TN values (Müller, 1977), and a wide range in particularly the vascular C_3 and C_4 end-member compositions. We relied on three approaches to lessen these effects: (1) a large dataset of $\delta^{13}C$ and TOC/TN (Fig. 5), which reduces the importance of individual data that might be influenced by NH_4^+ adsorption, (2) the additional less explored provenance proxy of Br/TOC, and (3) Monte Carlo simulations to reflect the influence of uncertainty in end-member compositions. We chose to use $\delta^{13}C_{TOC}$ as the main proxy for C_3–C_4 transition because the ease of the analytical procedure facilitates the gathering of a large dataset, and indeed, the $\delta^{13}C_{TOC}$ shows substantial scatter for nearly all time intervals, which suggest that restricted datasets using a more analytically challenging technique such as compound-specific isotope measurements may not fully reflect the range of isotopic variability during a given time interval.

While we used TOC/TN, measured on all samples, as the main proxy for organic matter provenance, we also analysed the trace element composition of a subset of samples (Figs. 4, 6; Table S2) to use Br/TOC as an additional proxy. The Br/TOC ratio in sediments with predominantly marine organic matter has been shown to far exceed that of sediments rich in terrigenous organic matter (Mayer *et al.* 2007), presumably due to the incorporation of Br-rich secondary metabolites produced by marine organisms (e.g. Gribble, 1998). Therefore, as Mayer *et al.* (2007) found, we expect a graph of $\delta^{13}C_{TOC}$ and Br/TOC to be consistent with mixing between three extreme end-member compositions, and Fig. 5 confirms this, though samples from IODP Site U1480 are not as Br-rich as those Mayer *et al.* (2007) analysed from continental shelf cores. To evaluate the potential of Br/TOC ratios as an indicator of

https://doi.org/10.1017/S0016756823000481 Published online by Cambridge University Press

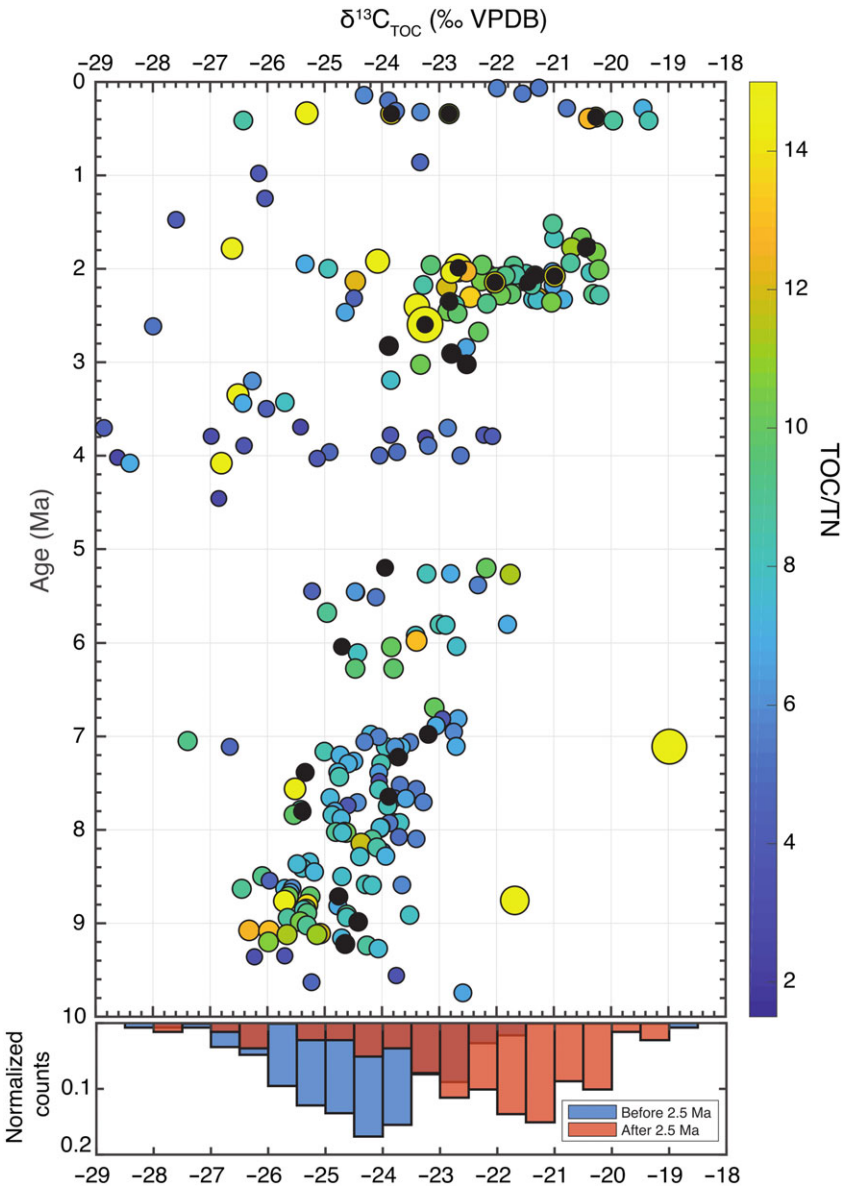

Figure 5. (Colour online) IODP Site U1480 $\delta^{13}C_{TOC}$ record for the past 10 Ma data with data points sized and coloured to reflect TOC/TN ratios, and black points indicating the subset of samples chosen for trace element analysis to establish Br/TOC. Higher (less negative) $\delta^{13}C$ values (permille, VPDB) imply greater contributions of terrestrial C4 or marine organic matter. The marginal histogram shows the difference in frequency of $\delta^{13}C_{TOC}$ before and after ~2.5 Ma.

Table 1. End-member values and ranges used in mixing models

End-member	$\delta^{13}C_{TOC}$ (‰ VPDB)	TOC/TN	Br/TOC (parts per thousand)
Terrigenous C_4	−14 to −16	8 to 30[a]	0.005 to 0.2
Terrigenous C_3	−25 to −30	8 to 30[a]	0.005 to 0.2
Marine	−18 to −23[b]	2 to 8	6 to 9

[a]The precise end-member composition range makes little difference in the final interpretation (see Supplemental Discussion).
[b]The effects of marine $\delta^{13}C$ end-member composition are considered in Section 4.1 and Fig. 6.

organic matter provenance in open ocean settings like Site U1480, we estimated the fraction of C_4 plant coverage using $\delta^{13}C$ and Br/TOC data to compare with results using the $\delta^{13}C$ and TOC/TN system (Fig. 6). The degree of agreement between these two methods depends heavily on the choice of marine end-member Br/TOC, but using the ~6–10 range suggested in Mayer *et al.* (2007) produces results that are remarkably similar to those generated using TOC/TN ratios. While the two methods of correcting for marine organic matter contributions are not entirely independent (both rely on $\delta^{13}C_{TOC}$ data), the agreement between the results they produce is encouraging.

We also used Monte Carlo simulations to help account for the uncertainty in C_4 abundance arising from the possible range of end-member composition. Figure 6 shows the results using 10^5 end-member compositions for $\delta^{13}C_{TOC}$, TOC/TN and Br/TOC taken randomly from distributions centred at our estimated end-member compositions and with generous standard deviations (Table 1). Because of the scatter in the resulting data, we used a bootstrapping technique to produce a range and best estimate (the resulting distribution median) of a smoothed curve of inferred C_4 landcover (Fig. 6). In general, the raw $\delta^{13}C_{TOC}$ record and the inferred C_4 coverage after correction for marine organic inputs show similar behaviour, suggesting that the overall influence of marine organic matter on reconstructions of landscape evolution is small, which accords with the correlation between vascular plant biomarker $\delta^{13}C$ and $\delta^{13}C_{TOC}$ that has been established previously (Freeman & Colarusso, 2001; Galy *et al.* 2008). However, while the

https://doi.org/10.1017/S0016756823000481 Published online by Cambridge University Press

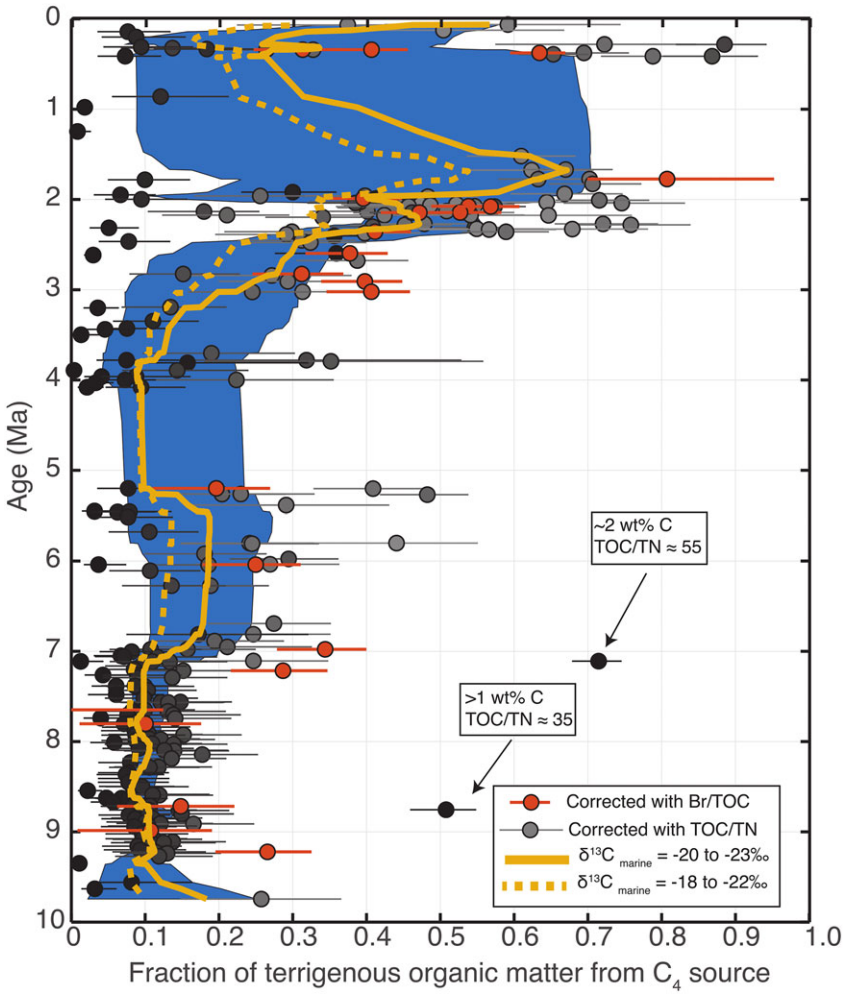

Figure 6. (Colour online) Estimated fraction of terrigenous organic matter from C_4 plants through time based on $\delta^{13}C_{TOC}$, TOC/TN and Br/TOC data from IODP Site 1480. Two separate mixing models using TOC/TN and Br/TOC data, respectively, were used to minimize the influence of marine organic matter. Data points in grey show the median output from 10^5 Monte Carlo simulations using random perturbations of TOC/TN and $\delta^{13}C_{TOC}$ end-member compositions, while the uncertainty bars represent the interquartile range of simulation outputs. Points in darker grey were inferred to have smaller contributions from marine organic matter and therefore underwent a smaller correction to minimize the influence of marine organic matter. Points in red show C_4 fraction when contributions to the $\delta^{13}C_{TOC}$ data from marine sources were corrected for using Br/TOC, and the error bars represent the interquartile of values based on Monte Carlo simulations. The blue region represents the interquartile range of smoothed curves resulting from random resampling (bootstrapping) of C_4 coverage estimates, while the yellow curve is the median of the smoothed curves from bootstrap resampling. Two main periods of C_4 expansion (~8.5–7 and ~2.5 Ma) are apparent, suggesting a multi-phase transition towards greater aridity.

$\delta^{13}C_{TOC}$ suggests that C_4 expansion (associated with increasing $\delta^{13}C_{TOC}$) may have started ~9 Ma, inferred C_4 coverage begins increasing just prior to 7 Ma. The fraction of organic matter from marine sources appears to have increased between 9 and 7 Ma, which causes the magnitude of the marine organic matter correction to increase during this interval and the inferred C_4 coverage to remain nearly constant.

4.a.1. Difficulty in estimating end-member compositions

Determining a reasonable range for the $\delta^{13}C$ composition of the marine organic end-member is particularly challenging because the data do not appear to uniformly support a $\delta^{13}C$ of ~−18 to −22 ‰ that the sea surface temperatures at this site would imply for phytoplankton (Descolas-Gros & Fontugne, 1990). Samples from IODP Site U1480E cores 1–2 largely post-date Nicobar Fan deposition and would therefore be expected to record the $\delta^{13}C$ of marine organic matter. Indeed, these samples average −21.8 ‰ (ignoring the −26.2 ‰ value for U1480E-2H-6 139–140 cm as unrealistic for pure marine organic matter). However, sediments that pre-date the Nicobar Fan, below about 1,250 m, and which should also record a relatively pristine marine $\delta^{13}C$ signal, have an average $\delta^{13}C$ of −25.3 ‰ with only two samples exceeding −23 ‰. This raises the possibility that the $\delta^{13}C$ of modern marine organic matter may not be valid as an end-member composition for samples from deeper in the core that underwent early diagenesis. The mechanism by which organic matter may become depleted in ^{13}C is not immediately clear, since processes such as methanogenesis would be expected to leave an organic residue highly enriched in ^{13}C. However, as Macko *et al.* (1994) discuss, degradation of organic matter, particularly protein-rich marine material, could lead to ^{13}C depletion of the residue due to a diverse set of reactions and associated fractionations available to more functionalized organic compounds. Because of this apparent discrepancy between C isotope compositions of marine organic matter, we tested the effects of using two different $\delta^{13}C$ ranges on the model outputs (Fig. 6). In one run, there are two models for C_3 and C_4 plant coverage: one using a marine organic matter $\delta^{13}C$ of −20 to −23 ‰, representing the highest values in sediments that underlie Nicobar Fan material, and a second using a $\delta^{13}C$ of −18 to −21% to reflect modern value phytoplankton $\delta^{13}C$ in appropriately warm regions (Descolas-Gros & Fontugne, 1990). The model results using the modern phytoplankton $\delta^{13}C$ suggest a lower fraction of C_4 coverage at all times during the past and a smaller initial episode of C_4 expansion commencing ~7 Ma. We are hesitant to ascribe inordinate physical meaning to the apparent decrease in C_4 coverage at ~5 Ma due to the data sparsity, primarily resulting from low coring recovery, between ~4 and 5 Ma. Because the main differences in inferred C_4 coverage lie in the earlier part of the record, it is likely that the first model run with $\delta^{13}C$ of marine organic matter reflecting the $\delta^{13}C$ of hemipelagic/pelagic

https://doi.org/10.1017/S0016756823000481 Published online by Cambridge University Press

sediments underlying the Nicobar Fan is more likely to accurately reflect the true C_4 plant coverage.

4.b. Strengths of the Nicobar Fan record

Part of the benefit of using terrigenous seafloor sediments such as those of the Nicobar Fan at IODP Site U1480 is that they spatially integrate heterogeneous signals over a wide enough area that localized changes are less likely to alter continental-scale interpretations. However, sediment records from the Bengal Fan may not fully archive terrestrial conditions during this time interval as the Nicobar Fan appears to have received a substantially greater fraction of Himalayan-sourced sediment (Pickering *et al.* 2019, 2020); therefore, IODP Site U1480 may be better suited for understanding C_4 expansion. Additionally, the analytical facility of conducting bulk TOC $\delta^{13}C$ analyses compared to compound-specific isotope measurements means that the average temporal resolution of our dataset is over ten times greater than that of biomarker $\delta^{13}C$ records from Freeman and Colarusso (2001) and Karp *et al.* (2018). The $\delta^{13}C_{TOC}$ record from IODP Site U1480 may therefore reveal trends and timing that are not apparent in lower-resolution biomarker datasets. Finally, analyses of terrestrial samples from specific formations like the well-studied Siwalik palaeosols (Fig. 1) may fail to capture the true onset of a transition that is spatially heterogenous on a continental scale. Indeed, the range in values of both $\delta^{13}C_{TOC}$ and inferred C_4 coverage during any given time interval in IODP Site U1480 record supports the hypothesis that the entire C_3–C_4 transition from ~7.1–2 Ma was patchy, and that local terrestrial samples or sparsely sampled compound-specific isotope records may not convey the full spatial variability in ecosystem composition (Vögeli *et al.* 2017).

Additionally, when compared with many studies using organic matter from sands/sandstones, the C_3–C_4 data presented in this study (from muds/mudstones) record a higher-resolution signal. Prior data from sandy sediments represent a more time-averaged response as these sediments can be stored in 'temporary sinks' in river and coastal systems for ~100 kyr or longer (Gaudemer & Metivier, 1999; Blöthe & Korup, 2013), complicating the correlation of sedimentary archives to climate forcing. Sandy beds tend to be much thicker than muds/mudstones and represent relatively infrequent events compared with muddy sediment delivery to ocean basins. Sand samples depend on the availability of coarser-grained sediment, especially compared with the abundance of finer-grained sediment. Even though plant material will also be stored with sands, to be incorporated into (relatively infrequent) SGFs, plant material is also supplied continuously to ocean basins via higher-frequency processes such as hyperpycnal flows, nepheloid layers and other plumes of suspended finer-grained sediment from river and coastal environments. Thus, understanding any climate change signals is best achieved by analysing muddy sediments from, for example, the distal parts of the Nicobar Fan. It is, therefore, perhaps unsurprising that many studies of sandy sediments tend to show more gradual (and temporally aliased) signals.

4.c. Climatic implications of inferred C_3–C_4 transition

Our data suggest that the expansion of C_4 plant coverage in the South Asia was punctuated by two distinct periods of C_4 expansion rather than a consistent gradual shift or single episode as inferred from many terrestrial and marine records (Quade *et al.* 1989; Prell & Kutzbach. 1992; Freeman & Colarusso, 2001; Gupta & Thomas, 2003). We infer an initial episode of C_4 expansion starting at ~7.1 Ma, which broadly agrees with the timing inferred from earlier studies (e.g. Bengal Fan $\delta^{13}C$ in Quade *et al.* 1989; $\delta^{13}C$ in Freeman & Colarusso, 2001) as well as a period of monsoon intensification (Rea *et al.* 1998; Wan *et al.* 2007) but slightly post-dates the inferred intensification of summer monsoon wind patterns from the Indian subcontinent (e.g. $\delta^{18}O$ from Quade *et al.* 1989) and Indian Ocean (Kroon *et al.* 1991; Prell & Kutzbach. 1992; Gupta & Thomas, 2003), in addition to the shift towards C_4 plant dominance in North America, South America and East Africa (Cerling *et al.* 1997). The second period of C_4 expansion beginning at ~3.5 Ma and punctuated by a rapid increase at ~2.5 Ma is inferred to be of greater magnitude and does not appear in records from either terrestrial palaeosols or marine sediments from the Bengal Fan, though the temporal resolution of these records is typically of insufficient resolution during this time interval. Using geochemical and magnetic data obtained from a ferromanganese crust in the western Pacific, together with climate models, Zhong *et al.* (2022) interpret their data to suggest an equatorward shift of the westerly jet and humidification of Central Asia during the gradual transition from a warm Pliocene climate to the cool Pleistocene, between ~2.5 and 2.7 Ma. This time interval coincides with our inferred increase in C_4 coverage (Fig. 7). Lu *et al.* (2020) used a temporally highly resolved (~500 years) sedimentological record from the Qaidam Basin, NE Tibetan Plateau, to show pronounced glacial–interglacial climate variability during the interval from 2.7 to 2.1 Ma.

4.c.1. First episode of C_4 expansion ~7.1 Ma

The first episode of C_4 expansion ~7.1 Ma appears to coincide with the timing of a period of monsoon intensification recorded in aeolian dust flux in the North Pacific (Rea *et al.* 1998) and South China Sea (Wan *et al.* 2007) and also agrees well with the timing of $\delta^{13}C$ increase in carbonate nodules from the Siwalik palaeosols. The decrease in median inferred C_4 coverage from ~5.5–5 Ma also mirrors the decrease in dust flux, though the gap in the IODP Site U1480 record from ~4.1–5.1 Ma makes us cautious in this interpretation. This episode of C_4 expansion in IODP Site U1480 record appears to pre-date the increase in $\delta^{13}C$ of vascular plant biomarkers that is apparent around 6 Ma (Freeman & Colarusso, 2001; Karp *et al.* 2018; Fig. 6), although there are difficulties in dating C_4 expansion using the compound-specific datasets that are discussed in Section 3.2. Interestingly, the initial pulse in dust flux to sites 885/886 at ~7.7 Ma does not coincide with either a change in soil carbonate $\delta^{18}O$, an indication of local monsoon intensity, or the first episode of C_4 expansion, although Rea *et al.* (1998) note that attributing a cause to this peak in dust flux is difficult.

Other records of monsoon intensity inferred from the loess plateaus suggest that aridification progressed northward through time as the East Asian monsoon intensified, increasing the difference in seasonal precipitation (Shen *et al.* 2017, 2018), which is consistent with our results. We detect the C_4 shift beginning ~7.1 Ma (*cf.* the 7.4–7.2 Ma expansion of C4 grasslands on the Indian subcontinent as documented from the Indus Fan, Arabian Sea, by Feakins *et al.* 2020), which lags slightly behind the change in Indian Ocean monsoon intensity inferred from carbonate nodule $\delta^{18}O$ (Freeman & Colarusso, 2001) but is contemporaneous with the increase in soil carbonate $\delta^{13}C$ of Quade *et al.* (1989). Additionally, northward C_4 grassland expansion is consistent with the shift towards higher $\delta^{13}C$ of mammal tooth enamel, which indicates a diet including more C_4 grasses, shortly after 10 Ma in northern Pakistan but later in China (Arppe *et al.* 2015).

https://doi.org/10.1017/S0016756823000481 Published online by Cambridge University Press

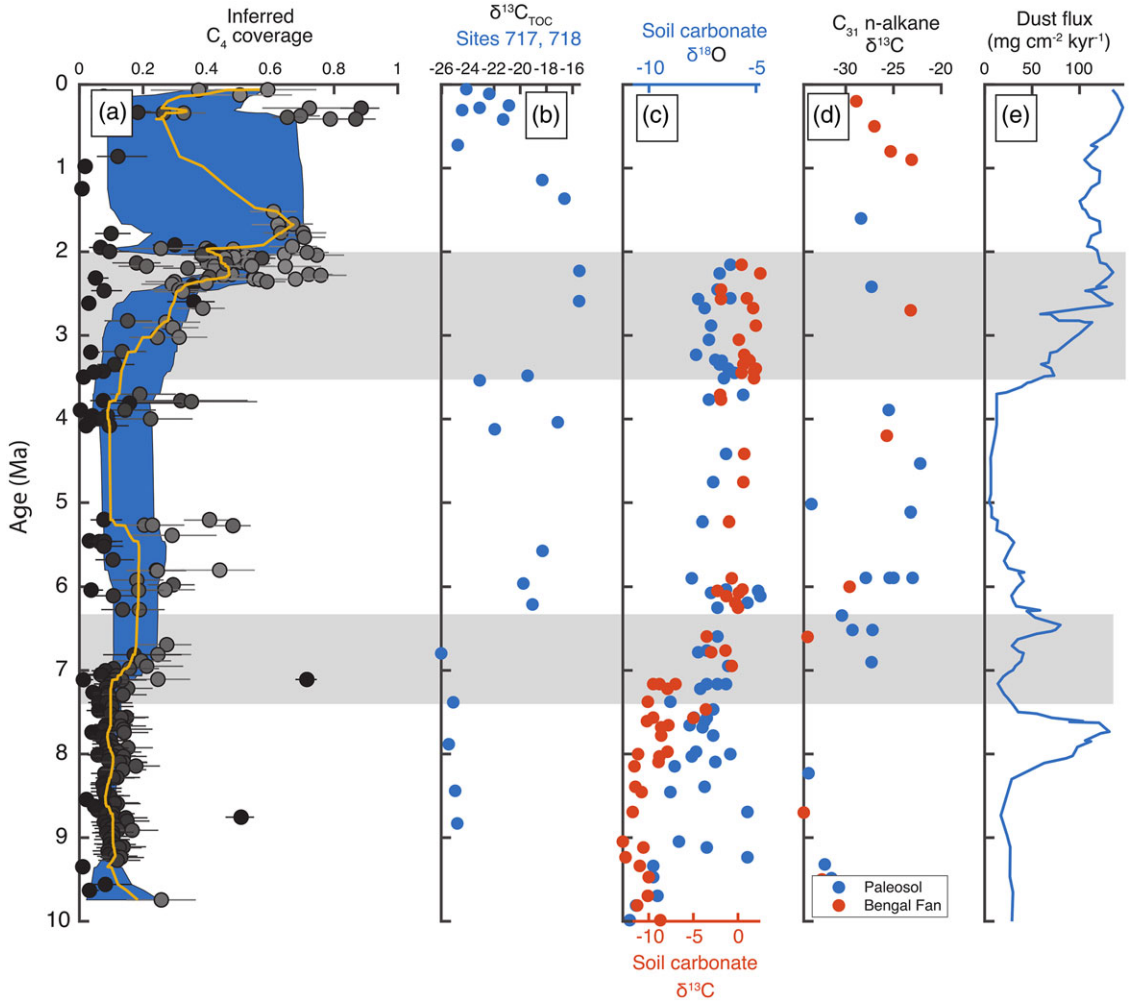

Figure 7. (Colour online) Comparison of multiple marine and terrestrial proxies for the C_3–C_4 changes and aridity including: (a) inferred C_4 coverage from IODP Site U1480 data (this study), (b) $\delta^{13}C_{TOC}$ from ODP sites 717 and 718 on the Bengal Fan (France-Lanord & Derry, 1994), (c) isotopic composition of carbonate nodules from the western Siwalik (Quade *et al.* 1989) with $\delta^{13}C$ and $\delta^{18}O$ relative to PDB, (d) $\delta^{13}C$ of C_{31} n-alkanes extracted from Siwalik palaeosols and Bengal Fan sediments (Freeman & Colarusso, 2001; Karp *et al.* 2018), and (e) dust flux at ODP sites 885 and 886 (Rea *et al.* 1998) in the North Pacific. The two periods of major C_4 expansion beginning at ~7 and 3.5 Ma in the IODP Site U1480 records are highlighted in grey.

However, we note that two samples (U1480G-42R-1 12–13 cm and U1480F-96X-1 18–19 cm) show a combination of high TOC (above 1 wt% C), high TOC/TN (~35 and 57, respectively) and $\delta^{13}C$ values of −19.0 and −21.7‰ at 8.8 and 7.1 Ma (Fig. 5), which strongly suggests localized areas of anomalously high C_4 coverage. This supports the 'vegetation mosaic' proposed by Freeman and Colarusso (2001) in which some environments like river floodplains are likely to be particularly sensitive to monsoon intensity as episodic inundation and desiccation would become more dramatic, favouring C_4 grasses that could resist drier winters. Monsoon intensification is likely, they argue, to have a lesser effect on more mountainous areas not susceptible to periodic flooding, and these environments are therefore more likely to retain C_3 plants. The modern landscape (Galy *et al.* 2008) and analyses of Siwalik palaeosol organic matter from the eastern front of the Himalaya (Vögeli *et al.* 2017) support spatial heterogeneity in aridity and C_3 and C_4 plant coverage, as do palynological studies (Morley, 2018) and model results based on orographic effects (Boos & Kuang, 2010). These two samples indicating significantly higher C_4 coverage than the bulk of the dataset may then represent localized pockets of C_4 abundance prior to the regional expansion. This would be consistent with the globally synchronous expansion of C_4 plant coverage beginning ~9 Ma (Kroon *et al.* 1991; Prell & Kutzbach. 1992; Cerling *et al.* 1997) and may argue for a more widespread mechanism than intensification of the South Asian monsoon. However, without additional data to corroborate C_4 expansion starting ~9 Ma, we are cautious not to over-interpret the dataset.

The explanation by Cerling *et al.* (1997) that decreasing atmospheric pCO_2 in the late Miocene was a fundamental driver of global climate change is supported by later studies (e.g. Pagani *et al.* 2005; Beerling & Royer, 2011; Rae *et al.* 2021). Pagani *et al.* (2005) pointed out that 'the fall in pCO_2 likely allowed for a critical expansion of ice sheets on Antarctica and promoted conditions that forced the onset of terrestrial C_4 photosynthesis'.

Finally, expansive wildfires have been proposed as either a cause or result of C_4 grassland expansion (Scheiter *et al.* 2012), but while records of fire frequency have limited temporal resolution, they do not appear to show an increase that is consistent with the first episode of C_4 expansion starting at ~7.1 Ma (Karp *et al.* 2018). The complexity and multitude of explanations for increasing aridity in South and Central Asia make us hesitant to definitively

https://doi.org/10.1017/S0016756823000481 Published online by Cambridge University Press

attribute the first C_4 expansion to a single mechanism, but a consensus appears to be building around the primacy of monsoon intensification (e.g. An *et al.* 2005), which is consistent with our observations.

4.c.2. Second episode of C_4 expansion

The second main feature of both the $\delta^{13}C$ data and inferred C_4 coverage is a gradual increase in inferred C_4 coverage beginning at ~3.5 Ma and punctuated by a sharp increase in $\delta^{13}C_{TOC}$ and C_4 fraction at ~2.5 Ma, effectively coeval with the major expansion of Northern Hemisphere glaciation (e.g. Raymo *et al.* 1989). Similar changes have been recorded in the abundance of marine primary producers thought to be particularly responsive to upwelling intensity (Kroon *et al.* 1991; Prell & Kutzbach. 1992) as well as magnetic susceptibility and aeolian dust flux from loess and marine sediment deposits (Fig. 6; Rea *et al.* 1998). However, other records of C_4 expansion on the Indian subcontinent do not record an additional transition at ~2.5 Ma (Quade *et al.* 1989; Cerling *et al.* 1997; Freeman & Colarusso, 2001; Karp *et al.* 2018), though several of these records lack the data coverage to identify such a transition (Fig. 6). While the stepwise ~2.5 Ma transition in the IODP Site U1480 record could conceivably arise from a sudden change in sediment provenance rather than true C_4 expansion, zircon age spectra from IODP Site U1480 are inconsistent with major sediment provenance shifts (McNeill *et al.* 2017a).

The increase in C_4 coverage beginning around 3.5 Ma coincides with a pronounced increase in North Pacific dust flux (Fig. 7), perhaps suggesting that monsoon intensification may have been a primary factor in the second episode of C_4 expansion as well. Within the overall trend towards greater C_4 coverage is a sharp transition at ~2.5 Ma that is notable both for its magnitude and abruptness. While we note that quantitative estimates of C_4 coverage are more affected by changes in end-member composition than trends, the highest inferred C_4 fractions just prior to 2.5 Ma are ~50% compared with samples implying 80% C_4 coverage just after 2.5 Ma. This increase is of similar magnitude to the change throughout the entire rest of the record but occurs over about 0.5 Myr. The sample density is relatively low just prior to this event, but even the smoothed bootstrapping results – which will be much less sensitive to individual data points – imply a sharp transition at ~2.5 Ma, suggesting it is unlikely to arise as an artefact of sample density. Such a dramatic, essentially stepwise, change demands a similarly abrupt cause and coincides with the major expansion of Northern Hemisphere glaciation (e.g. Zachos *et al.* 2001), which made South and East Asian climates more arid (Shen *et al.* 2017, 2018). However, it could be argued that the overall increase in inferred C_4 coverage between ~3.2 and 1.7 Ma (Fig. 7) may have been more related to uplift of the Himalaya and Tibetan Plateau leading to increase aridity in the source area for the sediments. Our estimates of C_4 fraction agree remarkably well with those of An *et al.* (2005) based on modelling results assuming multiple episodes of Himalayan uplift and records of East Asian summer monsoon intensity, so we cannot discount the possibilities that regional uplift, a global climate shift and/or spatially complex landscape evolution conspired to produce the ecological changes apparent in the IODP Site U1480 record.

5. Conclusions

Altogether, the elemental and isotopic composition of organic matter at IODP Site U1480 provides an unusually complete insight of major climate shifts on the Indian subcontinent since ~10 Ma and suggests two distinct episodes of C_4 expansion in the source area for the sediments. The first, beginning ~7.1 Ma, coincides with a period of inferred monsoon intensification and agrees well with the timing of a shift in soil carbonate $\delta^{13}C$ but pre-dates the ~6 Ma shift inferred from compound-specific isotope studies of limited temporal resolution. Isolated samples prior to this hint at the possibility of earlier C_4 expansion in some areas, which may help reconcile the timing with the slightly earlier C_4 expansion, observed on multiple continents (Cerling *et al.* 1997). The second episode of C_4 expansion began at ~3.5 Ma and was punctuated by a rapid shift at ~2.5 Ma, consistent with a climatic alteration contemporaneous with the expansion of Northern Hemisphere glaciation, a major climatic event whose effects have not been identified in records of C_4 plant coverage on the Indian subcontinent. While it seems reasonable to see a significant change in the relative importance of C_3 and C_4 plants (*cf.* Sarangi *et al.* 2021) in response to global cooling at ~2.5 Ma, which coincides with the dramatic increased sediment accumulation rates (SARs) in the Nicobar Fan (Site U1480 in Pickering *et al.* 2019, Fig. 9), this shift in SARs appears not to observed in the Bengal Fan, probably because at that time sediment routing was predominantly to the east in the Nicobar Fan. The underlying reasons for both phases of C_4 expansion may be complex and different, for example, with the latter involving at least a contributory tectonic component due to the sustained uplift of the Himalaya and Tibetan Plateau. Our data from the deep sea for a multi-phased C_4 expansion on the Indian subcontinent are broadly in agreement with terrestrial data from the Indian Siwaliks.

The wide array and complexity of potential forcing mechanisms make drawing definitive conclusions about climate vs tectonic drivers challenging (*cf.* Lenard *et al.* 2020); however, the uniquely detailed record of $\delta^{13}C_{TOC}$ from IODP Site U1480 underscores the potential for both local factors (e.g. monsoon intensification) and global (expansion of Northern Hemisphere glaciation) ones in causing spatially heterogenous landscape evolution. Our approach shows the promise of combining voluminous analytically facile data, multiple proxies and uncertainty estimation techniques to more quantitatively describe geochemical processes that can be linked to environmental change.

Supplementary material. The supplementary material for this article can be found at https://doi.org/10.1017/S0016756823000481

Acknowledgements. Participation on IODP Expedition 362 and post-expedition analyses were supported by the United States Science Support Program and the UK Natural Environment Research Council (NERC). Funding support was provided by the United States Science Support Program Post Expedition Award GG009393-01 to BMH. Dyke Andreasen and Colin Carney of the University of Santa Cruz Stable Isotope Laboratory provided insight into sample preparation and conducted analyses of organic matter. Sarah Feakins of the University of Southern California provided helpful discussion regarding sample preparation and data interpretation. We are particularly grateful to Marta Torres for her guidance and advice during IODP Expedition 362 and for enabling the INAA analyses. All members of the IODP Expedition 362 Scientific Party contributed to sample collection and generation of peripheral datasets. We thank Sarah Feakins, Peter Clift and an anonymous reviewer for their insightful comments in the review process that have led to a much improved manuscript.

References

An Z, Huang Y, Liu W, Guo Z, Clemens S, Li L, Prell W, Ning Y, Cai Y, Zhou W, Lin B, Zhang Q, Cao Y, Qiang X, Chang H and Wu Z (2005) Multiple expansions of C_4 plant biomass in East Asia since 7 Ma coupled with

strengthened monsoon circulation. *Geology* **33**, 705–8. https://doi.org/10.1130/G21423.1

Arppe L, Kaakinen A, Passey B, Zhang Z and Fortelius M (2015) Small mammal tooth enamel carbon isotope record of C_4 grasses in late Neogene China. *Global Planetary Change* **133**, 288–97. https://doi.org/10.1016/j.gloplacha.2015.09.003

Basu S, Agrawal S, Sanyal P, Mahato P, Kumar S and Sarkar A (2015) Carbon isotopic ratios of modern C3–C4 plants from the Gangetic Plain, India and its implications to paleovegetational reconstruction. *Paleogeography, Paleoclimatology, Paleoecology* **440**, 22–32.

Beerling DJ and Royer DL (2011) Convergent Cenozoic CO_2 history. *Nature Geoscience* **4**, 418–20.

Bianchi TS, Cui X, Blair NE, Burdige DJ, Eglinton TI and Galy V (2018) Centers of organic carbon burial and oxidation at the land-ocean interface. *Organic Geochemistry* **115**, 138–55.

Blöthe JH and Korup O (2013) Millennial lag times in the Himalayan sediment routing system. *Earth and Planetary Science Letters* **382**, 38–46. https://doi.org/10.1016/j.epsl.2013.08.044

Boos W and Kuang Z (2010) Dominant control of the South Asian monsoon by orographic insulation versus plateau heating. *Nature* **463**, 218–23. https://doi.org/10.1038/nature08707

Cerling T, Harris J, McFadden B, Leakey M, Quade J, Eisenmann V and Ehleringer J (1997) Global vegetation change through the Miocene/Pliocene boundary. *Nature* **389**, 153–8.

Chen W-H, Yan Y, Clift PD, Carter A, Huang C-Y, Pickering KT, Chemale Jr F, Shan Y and Zhang X (2020) Drainage evolution and exhumation history of the eastern Himalaya: insights from the Nicobar Fan, northeastern Indian Ocean. *Earth and Planetary Science Letters* **548**. https://doi.org/10.1016/j.epsl.2020.116472

Clift PD, Hodges KV, Heslop D, Hannigan R, van Long H and Calves G (2008) Correlation of Himalayan exhumation rates and Asian monsoon intensity. *Nature Geoscience* **1**, 875–80.

Curray JR (2014) The Bengal depositional system: from rift to orogeny. *Marine Geology* **352**, 59–69.

Descolas-Gros C and Fontugne M (1990) Stable carbon isotope fractionation by marine phytoplankton during photosynthesis. *Plant, Cell and Environment* **13**, 207–18.

Ding L, Kapp P, Cai F, Garzione CN, Xiong Z, Wang H and Wang C (2022) Timing and mechanisms of Tibetan Plateau uplift. *Nature* **3**, 652–67.

Dunlea AG, Giosan L and Huang Y (2020) Pliocene expansion of C4 vegetation in the Core Monsoon Zone on the Indian Peninsula. *Climates of the Past* **16**, 2533–46.

Edwards EJ, Osborne CP, Strömberg CAE, Smith SA and C4 Grasses Consortium (2010) The origins of C4 grasslands: integrating evolutionary and ecosystem science. *Science* **328**, 587–91. https://doi.org/10.1126/science.1177216

Expedition 354 Scientists (2016a) Site U1450. *Proceedings of the International Ocean Discovery Program* **354**. https://doi.org/10.14379/iodp.proc.354.105.2016

Expedition 354 Scientists (2016b) Site U1451. *Proceedings of the International Ocean Discovery Program* **354**. https://doi.org/10.14379/iodp.proc.354.105.2016

Expedition 354 Scientists (2016c) Site U1455. *Proceedings of the International Ocean Discovery Program* **354**. https://doi.org/10.14379/iodp.proc.354.105.2016

Feakins SJ, Liddy HM, Tauxe L, Galy V, Feng X, Tierney JE, Miao Y and Warny S (2020) Miocene C_4 grassland expansion as recorded by the Indus Fan. *Paleoceanography, Paleoclimatology* **35**, e2020PA003856.

France-Lanord C and Derry L (1994) δ13C of organic carbon in the Bengal Fan: Source evolution and transport of C3 and C4 plant carbon to marine sediments. *Geochimica Cosmochimica Acta* **58**, 4809–4814.

Freeman KH and Colarusso LA (2001) Molecular and isotopic records of C_4 grassland expansion in the late Miocene. *Geochimica Cosmochimica Acta* **65**, 1439–54.

Galy V, France-Lanord C and Lartiges B (2008) Loading and fate of particulate organic carbon from the Himalaya to the Ganga-Brahmaputra delta. *Geochimica Cosmochimica Acta* **72**, 1767–87.

Galy V, François L, France-Lanord C, Faure P, Kudrass H, Palhol F and Singh SK (2008) C_4 plants decline in the Himalayan basin since the Last Glacial maximum. *Quaternary Science Reviews* **27**, 1396–409. https://doi.org/10.1016/j.quascirev.2008.04.005

Gaudemer Y and Metivier F (1999) Stability of output fluxes of large rivers in South and East Asia during the last 2 million years: implications on floodplain processes. *Basin Research*. https://doi.org/10.1046/j.1365-2117.1999.00101.x

Gribble GW (1998) Naturally occurring organohalogen compounds. *Accounts of Chemical Research* **31**, 141–52. https://doi.org/10.1021/ar9701777

Gupta AK and Thomas E (2003) Initiation of Northern Hemisphere glaciation and strengthening of the northeast Indian monsoon: ocean Drilling Program Site 758, eastern equatorial Indian Ocean. *Geology* **31**, 47–50.

Hall R (2012) Late Jurassic-Cenozoic reconstructions of the Indonesian region and the Indian Ocean. *Tectonophysics* **570–571**, 1–41.

Karp A, Behrensmeyer A and Freeman KH (2018) Grassland fire ecology has roots in the late Miocene. *The Proceedings of the National Academy of Sciences (PNAS)* **115**, 1230–5.

Kennedy P, Kennedy H and Papadimitriou S (2005) The effect of acidification on the determination of organic carbon, total nitrogen and their stable isotopic composition in algae and marine sediment. *Rapid Communications in Mass Spectrometry* **19**, 1063–8.

Khim B-K, Lee J, Ha S, Park J, Pandey DK, Clift PD, Kulhanek DK, Steinke S, Griffith EM, Suzuki K, Xu Z and IODP Expedition 355 Scientists (2020) Variations in δ13C values of sedimentary organic matter since late Miocene time in the Indus Fan (IODP Site 1457) of the eastern Arabian Sea. *Geological Magazine* **157**, 1012–21. https://doi.org/10.1017/S0016756818000870

Kirkels FMSA, de Boer HJ, Concha Hernández P, Martes CRT, van der Meer MTJ, Basu S, Usman MO and Peterse F (2022b) Carbon isotopic ratios of modern C3 and C4 vegetation on the Indian peninsula and changes along the plant–soil–river continuum – implications for vegetation reconstructions. *Biogeosciences* **19**, 4107–4127. https://doi.org/10.5194/bg-19-4107-2022

Kirkels FMSA, Zwart HM, Usman MO, Hou S, Ponton C, Giosan L, Eglinton TI and Petersen F (2022a) From soil to sea: sources and transport of organic carbon traced by tetraether lipids in the monsoonal Godavari River, India. *Biogeosciences* **19**, 3979–4010.

Krishna MS, Naidu SA, Subbaiah CV, Sarma VVSS and Reddy NPC (2013) Distribution and sources of organic matter in surface sediments of the eastern continental margin of India. *Journal of Geophysical Research, Biogeosciences* **118**, 1484–94. https://doi.org/10.1002/2013jg002424

Kroon D, Steens T and Troelstra S (1991) Onset of Monsoonal related upwelling in the western Arabian Sea as revealed by planktonic foraminifers. *Proceedings of the Ocean Drilling Program Scientific Results* **117**, 257–63.

Lee H, Galy V, Feng X, Ponton C, Galy A, France-Lanord C and Feakins SJ (2019) Sustained wood burial in the Bengal Fan over the last 19 My. *Proceedings of the National Academy of Sciences* **116**, 22518–25.

Lenard SJP, Lavé J, France-Lanord C, Aumaître G, Bourlès DL and Keddadouche K (2020) Steady erosion rates in the Himalayas through late Cenozoic climatic changes. *Nature Geoscience* **13**, 448–52. https://doi.org/10.1038/s41561-020-0585-2

Lu Y, Dewald N, Koutsodendris A, Kaboth-Bahr S, Rösler W, Fang X, Pross J, Appel E and Friedrich O (2020) Sedimentological evidence for pronounced glacial-interglacial climate fluctuations in NE Tibet in the latest Pliocene to early Pleistocene. *Paleoceanography and Paleoclimatology* **35**, e2020PA003864. https://doi.org/10.1029/2020PA003864

Macko SA, Engels M and Qian Y (1994) Early diagenesis and organic matter preservation — a molecular stable carbon isotope perspective. *Chemical Geology* **114**, 365–79.

Mayer LM, Schick LL, Allison MA, Ruttenberg KC and Bentley SJ (2007) Marine vs. terrigenous organic matter in Louisiana coastal sediments: the uses of bromine:organic carbon ratios. *Marine Chemistry* **107**, 244–54. https://doi.org/10.1016/j.marchem.2007.07.007

McNeill LC, Dugan B, Backman J, Pickering KT, Pouderoux HFA, Henstock TJ, Petronotis KE, Carter A, Chemale F, Milliken KL, Kutterolf S, Mukoyoshi H, Chen W, Kachovich S, Mitchison FL, Bourlange S,

Colson TA, Frederik MCG, Guèrin G, Hamahashi M, House BM, Hüpers A, Jeppson TN, Kenigsberg AR, Kuranaga M, Nair N, Owari S, Shan Y, Song I, Torres ME, Vannucchi P, Vrolijk PJ, Yang T, Zhao X and Thomas E (2017a) Understanding Himalayan erosion and the significance of the Nicobar Fan. *Earth and Planetary Science Letters* **475**, 134–142. https://doi.org/10.1016/j.epsl.2017.07.019

McNeill LC, Dugan B, Petronotis KE and Expedition 362 Scientists (2017b) Site U1480. *In: Proceedings of the International Ocean Discovery Program*. https://doi.org/10.14379/iodp.proc.362.103.2017

Morley RJ (2018) Assembly and division of the South and South-East Asian flora in relation to tectonics and climate change. *Journal of Tropical Ecology* **34**, 209–34. https://doi.org/10.1017/S0266467418000202

Müller PJ (1977) C/N ratios in Pacific deep-sea sediments: effects of inorganic ammonium and organic nitrogen compounds sorbed by clays. *Geochimica Cosmochimica Acta* **41**, 765–76.

Pagani M, Zachos J, Freeman KH, Tipple B and Bohaty S (2005) Marked decline in atmospheric carbon dioxide concentrations during the Paleogene. *Science* **309**, 603–7. https://doi.org/10.1126/science.1110063

Pickering KT and Hiscott RN (2016) *Deep Marine Systems: Processes, Deposits, Environments, Tectonics and Sedimentation*. Oxford, UK: John Wiley & Son, 672 pp. ISBN: 978-1-4051-2578-9

Pickering KT, Pouderoux H, McNeill LC, Backman J, Chemale F, Kutterolf S, Milliken K, Mukoyoshi H, Henstock TJ, Stevens DE, Parnell C and Dugan B (2019) Sedimentology, stratigraphy and architecture of the Nicobar Fan (Bengal–Nicobar Fan System), Indian Ocean: results from International Ocean Discovery Program Expedition 362. *Sedimentology* **67**, 2248–81. https://doi.org/10.1111/sed.12701

Pickering KT, Carter A, Andò S, Garzanti E, Limonta M, Vezzoli G and Milliken K (2020) Deciphering relationships between the Nicobar and Bengal Submarine Fans, Indian Ocean. *Earth and Planetary Science Letters* **544**. https://doi.org/10.1016/j.epsl.2020.116329

Polissar PJ, Uno KT, Phelps SR, Karp AT, Freeman KH and Pensky JL (2021) Hydrologic changes drove the late Miocene expansion of C4 Grasslands on the Northern Indian subcontinent. *Paleoceanography, Paleoclimatology* **36**, e2020PA004108.

Prell WL and Kutzbach JE (1992) Sensitivity of the Indian monsoon to forcing parameters and implications for its evolution. *Nature* **360**, 647–52.

Quade J, Cerling T and Bowman J (1989) Development of Asian monsoon revealed by marked ecological shift during the latest Miocene in northern Pakistan. *Nature* **342**, 163–6.

Rae JWB, Zhang YG, Liu X, Foster GL, Stoll HM and Whiteford RDM (2021) Atmospheric CO_2 over the past 66 million years from marine archives. *Annual Review of Earth and Planetary Sciences* **49**, 609–41.

Raymo ME, Ruddiman WF, Backman J, Clement BM and Martinson DG (1989) Late Pliocene variation in northern hemisphere ice sheets and North Atlantic deep water circulation. *Paleoceanography* **4**, 413–46.

Rea DK, Snoeckx H, Joseph LH and Arbor A (1998) Late Cenozoic eolian deposition in the North Pacific: Asian drying, Tibetan uplift, and cooling of the northern hemisphere. *Paleoceanography* **13**, 215–24.

Roy B, Ghosh S and Sanyal P (2020) Morpho-tectonic control on the distribution of C_3-C_4 plants in the central Himalayan Siwaliks during Late Plio-Pleistocene. *Earth and Planetary Science Letters* **535**, 116119.

Sarangi V, Agrawal S and Sanyal P (2021) The disparity in the abundance of C_4 plants estimated using the carbon isotopic composition of paleosol components. *Paleogeography, Paleoclimatology and Paleoecology* **561**, 110068.

Scheiter S, Higgins S, Osborne C, Bradshaw C, Lunt D, Ripley B, Taylor L and Beerling D (2012) Fire and fire-adapted vegetation promoted C_4 expansion in the late Miocene. *New Phytologist* **195**, 653–66. https://doi.org/10.1111/j.1469-8137.2012.04202.x

Shen X, Wan S, Colin C, Tada R, Shi X, Pei W, Tan Y, Jiang X and Li A (2018) Increased seasonality and aridity drove the C_4 plant expansion in Central Asia since the Miocene–Pliocene boundary. *Earth and Planetary Science Letters* **502**, 74–83. https://doi.org/10.1016/j.epsl.2018.08.056

Shen X, Wan S, France-Lanord C, Clift PD, Tada R, Révillon S, Shi X, Zhao D, Liu Y, Yin X, Song Z and Li A (2017) History of Asian Eolian input to the Sea of Japan since 15 Ma: links to Tibetan uplift or global cooling? *Earth and Planetary Science Letters* **474**, 296–308. https://doi.org/10.1016/j.epsl.2017.06.053

Tauxe L and Feakins SJ (2020) A reassessment of the chronostratigraphy of late Miocene C3-C4 transitions. *Paleoceanography, Paleoclimatology* **35**, e2020PA003857.

Vögeli N, Najman Y, van der Beek P, Huyghe P, Wynn PM, Govin G, van der Veen I and Sachse D (2017) Lateral variations in vegetation in the Himalaya since the Miocene and implications for climate evolution. *Earth and Planetary Science Letters* **471**, 1–9. https://doi.org/10.1016/j.epsl.2017.04.037

Wan S, Li A, Clift PD and Stuut J-BW (2007) Development of the East Asian monsoon: mineralogical and sedimentologic records in the northern South China Sea since 20 Ma. *Palaeogeography, Palaeoclimatology, Palaeoecology* **254**, 561–82.

Zachos J, Pagani M, Sloan L, Thomas E and Billups K (2001) Trends, rhythyms, and aberrations in global climate 65 Ma to present. *Science* **292**, 686–93.

Zhisheng A, Kutzbach JE, Prell WL and Porter SC (2001) Evolution of Asian monsoons and phased uplift of the Himalaya-Tibetan plateau since Late Miocene times. *Nature* **411**, 62–6.

Zhong Y, Shi X, Yang H, Wilson DJ, Hein JR, Kaboth-Bahr S, Lu Z, Clift PD, Yan Q, Lohmann G, Liu J, González FJ, Jiang X and Liu Q (2022) Humidification of Central Asia and equatorward shifts of westerly winds since the late Pliocene. *Nature Communications, Earth and Environment*. https://doi.org/10.1038/s43247-022-00604-5

https://doi.org/10.1017/S0016756823000481 Published online by Cambridge University Press